Vol.7 No.4 Oct 2024

Journal of Networking and Communication Systems

Received 26 August, Revised 30 August, Accepted 15 October

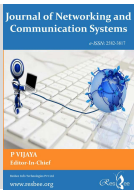

Local Gradient Arnold Transform-Deep Learning for Diabetic Retinopathy Detection Utilizing Retinal Fundus Image

K. Kalai Kumar

Associate Professor
Artificial Intelligence and Data Science
DMI College of Engineering, Chennai, Tamil Nadu
Mail id: kalaikumar23@gmail.com

Abstract: Diabetic retinopathy is one of the fundamental reasons for vision impairment globally. Early detection may eradicate the occurrence of severe vision loss and enhance the treatment efficacy. Moreover, fundus imaging is extensively employed to analyze diabetic retinopathy. Nevertheless, the accuracy of fundus imaging-based diagnosis is reliant on the skill of ophthalmologists. To bridge this gap, a module is introduced for diabetic retinopathy using retinal fundus image-enabled Local Gradient Arnold Transform-based Principal Component Analysis (LGAT-PCANet). An input retinal fundus image is performed for further processing. The image pre-processing is performed by Adaptive Wiener Filter (AWF). The optical disc segmentation is carried out using the Active Contour model and blood vessel segmentation is done by parking process, where these two segmentations are done with the help of a pre-processed image. The feature extraction is conducted with an input image and segmented image of the optical disc and blood vessel. Hence, diabetic retinopathy is detected by utilizing a Principal Component Analysis Network (PCANet). The metrics of LGAT-PCANet, such as accuracy, sensitivity, and specificity obtained 90.315%, 89.581%, and 91.489%.

Keywords: Diabetic Retinopathy, Retinal Fundus Image, Adaptive Wiener Filter, Arnold Transform, Local Gradient Pattern.

Nomenclature

Abbreviation	Expansion
AI	Artificial Intelligence
DL	Deep Learning
ML	Machine Learning
CNNs	Convolutional Neural Networks
LGP	Local Gradient Patterns
AVR	Artery to Vein Ratio
ADL-CNN	Active Deep Learning and CNN
DRNet13	Diabetic Retinopathy Network

1. Introduction

In the medical domain, the medical care of diseases is extremely effective when it is detected at an early phase. One of the main diseases is Diabetes, which increases the glucose amount in the blood due to inadequate insulin [7]. Due to the growth of diabetes, the disease tends to impact the circulatory system, which includes the retina, and ensues as long-term accumulated damage to blood vessels, decreasing the vision of patients led to diabetic retinopathy [8]. Currently, it is a life-threatening problem of diabetes mellitus owing to the increasing number of blindness all over the world [5]. The long duration of the occurrence of retinopathy will increase the risk of patients. This shows that diabetes patients are generally inattentive to DR possibility that might delay the treatment and diagnosis process. Manual detection of DR consumes more time and needs trained medical specialists to analyze digital color fundus images. Nevertheless, the delayed results may provide inadequate follow-up and misinformation for patients [6]. The retinal image obtained from the fundal camera provides helpful information based on the consequence and nature of the impact of diabetes on the eye. These images aid the ophthalmologist in evaluating the patients to plan several forms of management and monitor the process more effectively [8].

© Resbee Info Technologies Pvt Ltd
https://doi.org/10.46253/jnacs.v7i4.a5

Currently, detection approaches are observed by including a trained specialist manually identifying the vascular abnormalities as well as structural variations of the retina in the retinal fundus image. Based on automatic DR monitoring techniques, highly unreliable outcomes are identified from diverse readers, thus automated diagnosis modules of diabetic retinopathy are significant in resolving the issues [10]. Current developments in AI and the increase in computational resources created the prospect of designing DL applications for precise DR detection and classification [9]. DL is a subdivision of ML modules that is also a computer-aided medical diagnosis system, which includes hierarchical layers for unsupervised feature learning and classifying the patterns. The applications of DL related to image analysis involve segmentation, retrieval, detection, and classification of images. Presently, DL has been highly employed in the diabetic retinopathy detection process, which effectively learns the input data features even though more heterogeneous sources are incorporated. DL-based techniques, like Autoencoder, sparse coding, and CNNs are analyzed [7]. Therefore, this research introduces a module for diabetic retinopathy, since the performance of the model improved by increasing the training data and providing better reliability.

This model intends to present a diabetic retinopathy detection model with a retinal fundus image based on LGAT-PCANet. Here, an image attained from the dataset is pre-processed by employing AWF. Also, the optical disc segmentation process is conducted with an active contour model and blood vessel segmentation is done through the sparking process. Furthermore, feature extraction is carried out, wherein the extracted features are LGP with Arnold transform, AVR, entropy, and area. Therefore, diabetic retinopathy is detected by employing PCANet.

- **Proposed LGAT-PCANet for Diabetic Retinopathy Detection:** In this research, diabetic retinopathy detection is designed by a retinal fundus image named LGAT-PCANet. Here, a network named PCANet is considered for effectually detecting diabetic retinopathy.

The arrangement of this research is explicated as: In the second section, the brief review of conventional approaches is discussed; the third section elaborates on the methodology of this research; the fourth section briefs the outcomes performed in the following analysis; and the fifth section ends with future scope.

2. Motivation

Diabetic retinopathy is the leading cause of vision loss, where earlier prediction is the only solution to prevent vision loss. Recently, medical image processing of retinal fundus images has developed as a significant research domain for helping an ophthalmologist in medical diagnosis. So, the researchers are interested in designing a model by reviewing the preceding models.

2.1 Literature Survey

Ozbay, E., [1] introduced ADL-CNN in detecting diabetic retinopathy. This approach obtained maximal computational cost based on high-level data. Nevertheless, it did not employ rationally oriented color space for generating higher RGB color content from the images. Novitasari, D.C.R., *et al.* [2] designed CNN and Deep Extreme Learning Machine (CDELM) to detect diabetic retinopathy. The faster time of this model was maximum and it was more optimal than the other techniques. Nonetheless, it failed to compute the square matrix dimension due to the large amount of data.

Singh, S.P., *et al.* [3] developed pretrained EfficientNetB0 CNN for detecting diabetic retinopathy using fundus image. This approach effectively enhanced the performance of histogram equalization and channel extraction. However, it could not integrate existing systems due to the additional training, which may lead to more time.

Shamrat, F.J.M., *et al.* [4] presented the DRNet13 model to enhance diabetic retinopathy detection. This system demonstrated a better ability to identify significant features in a timely and accurate manner. However, this technique did not enhance the robustness by utilizing different data, which preserved an extensive range of diabetic retinopathy phases and patient demographics.

2.2 Challenges

The problems of traditional approaches are deliberated as,

- The model introduced in [1] was more robust by effectively optimizing the hyperparameters. However, the transformers method was not utilized which may allow to processing of multiple modalities utilizing parallel processing blocks with its simple design.
- An approach developed in [2] offered constant outcomes and reduced the variability that occurred with human interpretation. Nevertheless, the development and implementation costs were high and it consumed more time due to the usage of medical devices or software.

- Recently, Diabetic Retinopathy is a complicated disease based on diabetes, which becomes a threat to human life when it is not detected early. This affects the retina and the diagnosis is done by fundus image through several visions, which can be visualized. However, visual inspection is a complicated task and diagnosis relies on the expert. Thus, a new model for diabetic retinopathy is proposed in this research.

3. Proposed LGAT-PCANet for Diabetic Retinopathy Detection

Automatic prediction of lesions in retinal fundus images may be helpful for earlier detection of diabetic retinopathy. The goal of this investigation is based on detecting diabetic retinopathy disease with retinal fundus image using LGAT-PCANet. A retinal fundus image obtained from the database [20] is carried out to perform the image pre-processing phase, where the unwanted noise is deduced utilizing AWF [11]. Afterward, the pre-processed image is forwarded to segmentation of the optic disc and blood vessel phases, where it is performed using the active contour model [12] and sparking process [13] respectively. After that, the input image, and the two segmented images are subjected to the feature extraction phase, where the suitable feature vector is obtained. Here, the features considered are LGP [14] with Arnold transform [15], AVR [16], entropy [17], and area [18]. Thus, the detection of diabetic retinopathy is accomplished by utilizing PCANet [19]. Fig. 1 displays a schematic outline of diabetic retinopathy detection.

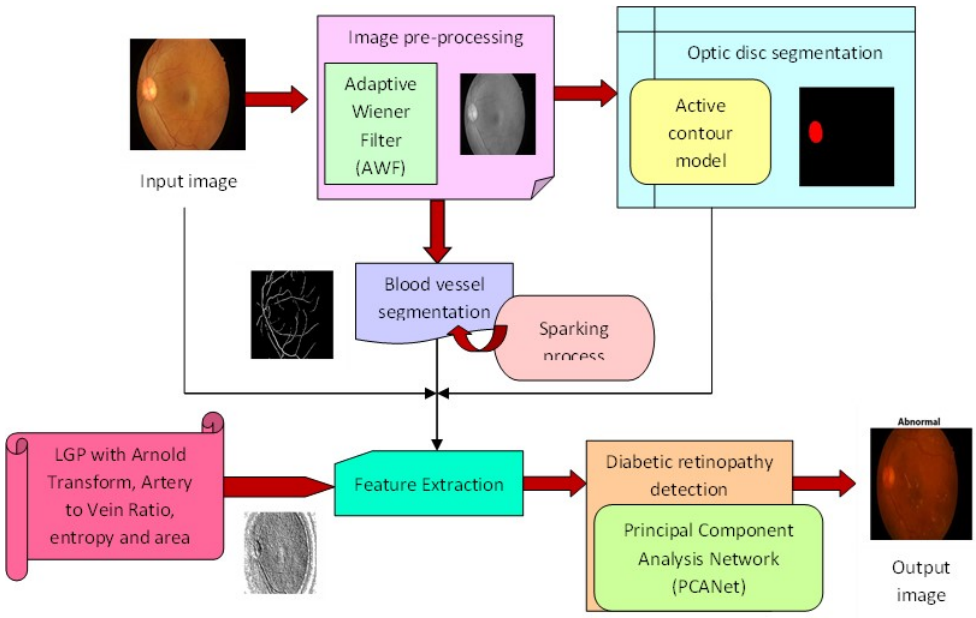

Fig. 1. *Schematic outline of diabetic retinopathy detection*

3.1 Image Acquisition

IDRiD [20] database has segmentation, disease grading, and localization phases, where the images in this dataset are in the JPG and CSV file format. It has both training and testing sets. Consider a database 'R' with 'h' count of retinal fundus images, which is articulated as

$$R = \left\{R_1, R_2, ...R_g, ...R_h\right\} \tag{1}$$

Here, R_g enumerates input images and R_h indicates the total number of images.

3.2 Image pre-processing using AWF

It is performed to eliminate inappropriate artifacts. Here, R_g is forwarded as an input to filter the image that is done using AWF.

3.2.1 AWF

It regulates the resultant of the filter [11] based on the local variance of an image and its significant objective is to reduce the error among restored and actual image. This filter is more accommodative to sustain edges and high-frequency regions. Thus, the below expression is determined for processing the pixels, which is modeled as,

$$W_g = \vartheta + (1 - b + \delta) * (R_g - \vartheta) \tag{2}$$

$$b = \frac{\kappa_{avg}}{\kappa_{\text{var}} + 1} \tag{3}$$

$$\delta = \frac{\kappa_{\text{var}}}{\kappa_{avg} + \kappa_{\max} + 1} \tag{4}$$

Here, W_g refers output pixel image which is the filtered image, R_g implies the input image, κ_{avg} indicates the mean of total pixels, κ_{var} represents the variance of the current pixel, and $\kappa_{\max}$ enumerates the maximal variance of overall images.

3.3 Optical Disc segmentation by Active contour model

It explicates the process of precisely defining and predicting optics from the neighboring retinal features in the eye image. Here, W_g is subjected as input for segmenting the optic disc utilizing an active contour model.

3.3.1 Active Contour Model

The active contour model [12] or snake is the major approach in the image segmentation process. The parametric active contours are employed in medical image analysis, which is also referred to as a closed parametric curve expressed by,

$$\partial_{med}(\mu, \nu) = \underset{(\mu,\nu)\in U_{\mu\nu}}{median} \{\partial(\mu, \nu)\} \tag{5}$$

Here, $k(\theta)$ specifies contour generated by cartesian coordinates $\mu(\theta)$ and $\nu(\theta)$ and θ is a factor where the coordinates are altered. The energy is significant for this process that is based on deformable contour. Thus, the power function of the snake is formulated using,

$$G_{snake} = \int_0^1 G_{snake}(k(\theta))\, d\theta \tag{6}$$

$$G_{snake} = \int_0^1 G_{in}(k(\theta)) + G_{img}(k(\theta)) + G_{cn}(k(\theta))\, d\theta \tag{7}$$

Here, G_{cn} defines energy attained by external constraint, G_{in} refers to internal energy, and G_{img} indicates energy based on image, where the expression of these energies are expressed below.

$$G_{in} = s(\theta)\left|\frac{\partial k}{\partial \theta}\right|^2 + \omega(\theta)\left|\frac{\partial^2 k}{\partial \theta^2}\right|^2 \tag{8}$$

$$G_{img} = o_{line} G_{line} + o_{edge} G_{edge} \tag{9}$$

$$G_{line} = O_{img}(\mu, \nu) \tag{10}$$

$$G_{edge} = -\left|\nabla O_{img}(\mu, \nu)\right|^2 \tag{11}$$

Here, $s(\theta)$ and $\omega(\theta)$ specifies the elasticity of curve and thickness of the curve, o implies weight. To eradicate the noise in the actual image and smoothen the edge, a Gaussian filter is used to enhance the capture range that is expressed as,

$$G_{edge} = -\left|G_\sigma(\mu, \nu) \times \nabla^2 O_{img}(\mu, \nu)\right|^2 \tag{12}$$

Here, $G_\sigma \times O_{img}$ depicts the convolution (conv) of the image O_{img} with a Gaussian kernel with a standard deviation of σ. Therefore, the segmented image of the optic disc is signified as A_g.

3.4 Blood vessel segmentation by sparking process

It is based on the process of isolating and identifying the blood vessels in the retina from neighboring tissues. Here, W_g is forwarded to segment the blood vessels by carrying out the sparking process.

3.4.1 Sparking process

The algorithm of the sparking process [13] for automatic blood vessel segmentation using the estimation of optimal threshold values. Consider χ as an arbitrary integer generated with $[1 \times \eta]$ and a_υ as the threshold value. The exponential kernel is found by transforming data into an exponential function, which is expressed by,

$$\ell_1 = \exp\left[\frac{\chi^2}{2a_\upsilon{}^2}\right] \tag{13}$$

The vector ℓ_1 is normalized for attaining the kernel that is modeled as,

$$\ell_1 = \frac{\left[\frac{1}{\eta}\sum_{\hbar=1}^{\eta}\max\left(\ell_1\right)-\ell_1\right]-\ell_1}{\sum_{\hbar=1}^{\eta}\max\left(\ell_1\right)-\ell_1} \tag{14}$$

The sparking image is determined by utilizing,

$$\lambda_{new}\left(\hbar,\lambda\right) = \frac{\lambda_\ell + \lambda_{\min(\hbar,\lambda)}}{\lambda_{\max(\hbar,\lambda)}} \tag{15}$$

where the values of $\lambda_{\min(\hbar,\lambda)}$ and $\lambda_{\max(\hbar,\lambda)}$ are $\lambda_{\min(\hbar,\lambda)} = \min\left[\Upsilon_1\left(\hbar,\lambda\right),\Upsilon_2\left(\hbar,\lambda\right),.....,\Upsilon_\eta\left(\hbar,\lambda\right)\right]$ and $\lambda_{\max(\hbar,\lambda)} = \max\left[\Upsilon_1\left(\hbar,\lambda\right),\Upsilon_2\left(\hbar,\lambda\right),.....,\Upsilon_\eta\left(\hbar,\lambda\right)\right]$. Therefore, the blood vessel segmented image is expressed as S_g.

3.5 Feature Extraction

It processes for eliminating the data dimension. Here, R_g, A_g and S_g are passed through the feature extraction phase. The features utilized in this process are explained below.

3.5.1 LGP with Arnold Transform

In this phase, A_g and R_g is subjected as an input for LGP for attaining the textural image, then the Arnold transform to obtain the feature vector F_1 and F_2.

a) LGP: It evaluates the gradient of pixel intensities in the local neighborhood, which aids in finding the edges and textures in an image [14], which is determined as,

$$LGP_{\psi,\mathrm{O}}^{\varpi,riu2} = \begin{cases}\sum_{r=0}^{\psi-1}\mathrm{M}^{\varpi}\left(y_r - y_{\mathrm{M}}\right) & if\ \mathrm{N}\left(LGP_{\psi,\mathrm{O}}^{\varpi}\right)\le 2\\ \psi+1 & else\end{cases} \tag{16}$$

Here, ψ signifies overall neighbors, O symbolizes neighbor's radius, y_r defines neighboring pixels, and N refers to a frequency between $\left[0,1\right]$. The textural feature attained from LGP is L_g, in which this is applied to the Arnold transform to attain a feature vector.

b) Arnold Transform: Arnold transform [15] may shift the pixel position rather than altering its values and it is frequently employed for image encryption and watermarking, which is modeled by,

$$\begin{pmatrix}X'\\Y'\end{pmatrix} = \begin{pmatrix}1 & 1\\2 & 2\end{pmatrix}\begin{pmatrix}X\\Y\end{pmatrix}\bmod \mathrm{P} \tag{17}$$

Here, $\begin{pmatrix}X'\\Y'\end{pmatrix}$ and $\begin{pmatrix}X\\Y\end{pmatrix}$ represents the image pixel's position vector after and before the shifting process, mod implies the modulus function, and P refers to the dimension of the target image utilized for determining the period of the Arnold transform.

Therefore, the feature vector obtained using A_g and R_g is symbolized as F_1 and F_2 respectively. Moreover, features like AVR, entropy, and area are applied over the blood vessel segmented image S_g to acquire a feature vector F_3.

3.5.2 AVR

It is computed by employing the largest arteries and veins on retinal images centered at the optic disc [16], which is modeled using,

$$o_1 = \frac{\sum_{c=0}^{f} Z_{\mathrm{K}c}/f}{\sum_{d=0}^{e} Z_{\mathrm{X}d}/e} \tag{18}$$

Here, the width of the artery and vein indicates $Z_{\mathrm{K}c}$ and $Z_{\mathrm{X}d}$, f and e explicates the number of arteries and veins and o_1 implies AVR.

3.5.3 Entropy

It is employed to estimate the impurity linked with arbitrary variables [17]. The entropy I of distinct value Z with probability mass function $\Re(Z)$ is modeled by,

$$o_2 = \mathrm{I}(Z) = -\sum_{g}^{h} \Re\left(S_g\right) \cdot \log_2 \Re\left(S_g\right) \tag{19}$$

Here, o_2 expresses entropy.

3.5.4 Area

It is defined as the overall pixels that create pattern objects in the binary image [18] that is expressed as,

$$o_3 = \sum_{(m,n)\in\Phi_\rho} 1 \tag{20}$$

Here, Φ_ρ enumerates a set of overall pixels generating ρ -object, (m,n) explicates pixels, and o_3 specifies area.

Thus, the feature vector F_3 is expressed as,

$$F_3 = \{o_1, o_2, o_3\} \tag{21}$$

Therefore, the resultant feature vector F_g is modeled by,

$$F_g = F_1 \| F_2 \| F_3 \tag{22}$$

3.6 Diabetic Retinopathy Detection using PCANet

Diabetic Retinopathy is a complicated disease that is a leading cause of vision loss and impairment. Exact prediction of DR stages may extremely enhance the intervention that eventually eradicates the risk of permanent vision loss. Therefore, PCANet is considered for detecting diabetic retinopathy with fundus image with the help of previous process output that is modeled as F_g, where its structure is explained below.

3.6.1 Structure of PCANet

Consider H number of input training images $\{J_i\}_{i=1}^{H}$ with $u \times v$ dimension, and patch size as $w_1 \times w_2$ at all phases [19]. Here, the PCA filters should learn from $\{J_i\}_{i=1}^{H}$. The phases of PCA are elaborated below.

a) First phase of PCA: Consider $w_1 \times w_2$ patch around every pixel and overlapping the patches of i^{th} image that are illustrated as $m_{i,1}, m_{i,2}, ..., m_{i,uv} \in \aleph^{w_1 w_2}$, in which every $m_{i,j}$ demonstrates j^{th} vectorized patch in J_i. After that, subtract the average of the patch from each patch and achieve $\overline{K_i} = \left\{\overline{m}_{i,1}, \overline{m}_{i,2}, ..., \overline{m}_{i,uv}\right\}$. Here, $\overline{m}_{i,j}$ expresses the average of the removed patch. While creating a similar matrix for entire input images is integrated, Eq. (23) is attained.

$$K = \left[\overline{K_1}, \overline{K_2}, ..., \overline{K_H}\right] \in \aleph^{w_1 w_2 \times H_{uv}} \tag{23}$$

Consider overall filters in the layer i as M_i PCA reduces the regeneration error in orthonormal filters that are illustrated as

$$\min_{E\in\aleph^{w_1 w_2 \times M_1}} \left\| K - EE^{Q}K \right\|_P^2, s.t. E^{Q}E = J_{M_1} \tag{24}$$

Here, J_{M_1} indicates the identity matrix of dimension $M_1 \times M_1$. The solution is defined as M_1 principal eigenvectors KK^{Q}. Thus, PCA filters are modeled as,

$$N_l^1 = mat_{w_1 w_2}\left(p_l\left(KK^{Q}\right)\right) \in \aleph^{w_1 \times w_2},\ l = 1, 2, ..., M_1 \tag{25}$$

Here, $mat_{w_1 w_2}$ indicates a function that maps $t \in \aleph^{w_1 w_2}$ to a matrix $N \in \aleph^{w_1 w_2}$ and $p_l\left(KK^{Q}\right)$ implies l^{th} the principal eigenvector KK^{Q}.

b) Second phase of PCA: Consider, l^{th} filter resultant of the initial phase as,

$$J_i^l = J_i * N_l^1,\ \ i = 1, 2, ..., H \tag{26}$$

Here, $*$ specifies 2D conv and boundary of J_i is zero-padded before convolving with N_l^1 for making J_i^l with J_i dimension. Consequently, gather overall patches J_i^l and subtract the average of patches, and generate

$\overline{V}_i^l = \left[\overline{n}_{i,l,1}, \overline{n}_{i,l,2}, ..., \overline{n}_{i,l,uv}\right] \in \aleph^{w_1 w_2 \times uv}$. Here, $\overline{n}_{i,l,j}$ is the j^{th} average of the removed patch in J_i^l. Moreover, $V^l = \left[\overline{V}_1^l, \overline{V}_2^l, ... \overline{V}_H^l\right] \in \aleph^{w_1 w_2 \times H_{uv}}$ for the matrix collecting the overall average of removed patches of l^{th} filter outcome and concatenate V^l for entire filter outcomes that are expressed by,

$$V = \left[V^1, V^2, ..., V^{M_1}\right] \in \aleph^{w_1 w_2 \times M_1 H_{uv}} \tag{27}$$

The PCA filters in this phase are determined by,

$$N_l^2 = mat_{w_1, w_2}\left(p_l\left(VV^Q\right)\right) \in \aleph^{w_1 \times w_1}, l = 1, 2, ... M_2 \tag{28}$$

For J_i^l, the resultant of M_2 is observed and every J_i^l is convolved with N_l^2 for $l = 1, 2, ..., M_2$, which is formulated as,

$$L_i^l = \left\{J_i^l * N_l^2\right\}_{l=1}^{M_2} \tag{29}$$

The number of outcomes attained from this stage is specified as M_1 M_2.

c) Output phase: Every input image M_1 for the previous phase has M_2 real-valued resultants $\left\{J_i^l * N_l^2\right\}_{l=1}^{M_2}$ from the previous phase. The outcomes are binarized and attained $\left\{B\left(J_i^l * N_l^2\right)\right\}_{l=1}^{M_2}$. Here, $B(\bullet)$ represents the Heaviside step function. In every pixel, the vector of M_2 binary bits is considered as a decimal number that converts M_2 outputs L_i^l as an integer value image that is formulated as,

$$Q_i^l = \sum_{l=1}^{M_2} 2^{l-1} B\left(J_i^l * N_l^2\right) \tag{30}$$

Every M_1 image then Q_i^l, $l = 1, 2, ... M_1$ is divided into C blocks. The histogram of decimal values in every block is computed and concatenates total C histograms into a vector that specifies $Bhist\left(Q_i^l\right)$. The feature of the input image H_i is referred to as the set of block-wise histograms after encoding that is modeled as,

$$\alpha_i = \left[Bhist\left(Q_i^l\right), ... Bhist\left(Q_i^{M_1}\right)\right]^Q \in \aleph^{(2M_2)M_1 C} \tag{31}$$

Here, w_1, w_2 signifies filter size, the number of filters in every phase is specified as M_1, M_2. Therefore, the detected outcome is specified as D_g. Fig. 2 demonstrates the structure of PCANet.

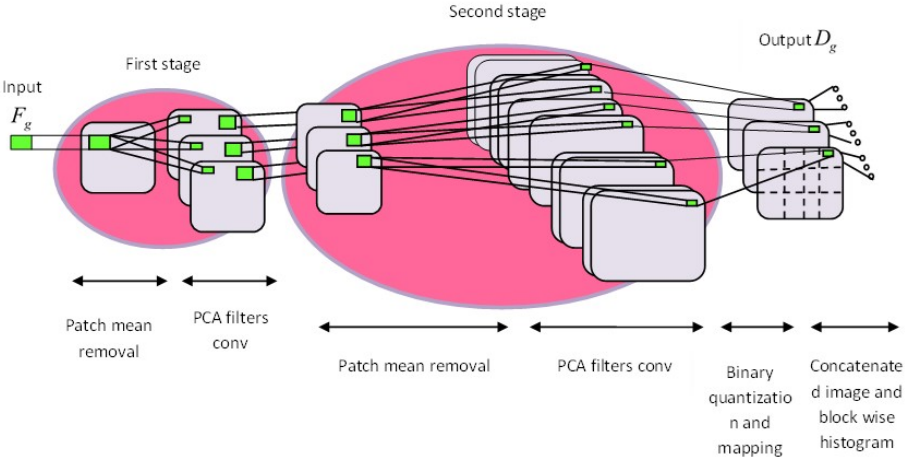

Fig. 2. *Structure of PCANet*

4. Results and Discussions

The sections describe the results and analysis of LGAT-PCANet.

4.1 Experimental Setup

LGAT-PCANet is implemented in PYTHON.

4.2 Experimental Outcomes

The image results are mentioned in Fig. 3 with the normal and abnormal images. Fig. 3 a) depicts input image-1, Fig. 3 b) enumerates input image-2, Fig. 3 c) demonstrates pre-processed image-1, Fig. 3 d) indicates pre-processed image-2, Fig. 3 e) depicts optic disc segmented image-1, Fig. 3 f) specifies optic disc segmented image-2, Fig. 3 g) signifies blood vessel segmented image-1, Fig. 3 h) indicates blood vessel segmented image-2, Fig. 3 i) depicts LGB feature image-1, Fig. 3 j) enumerates LGB feature image-2, Fig. 3 k) demonstrates detected image-1, Fig. 3 l) indicates detected image-2.

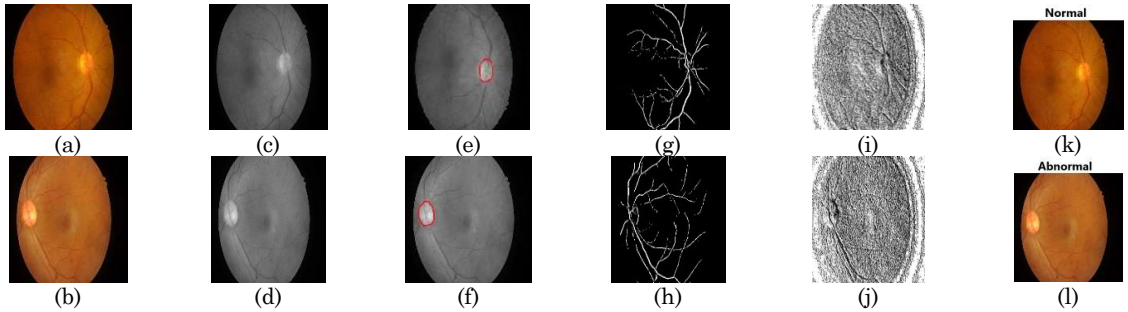

Fig. 3. *Image results of LGAT-PCANet, a) input image-1, b) input image-2, c) pre-processed image-1, d) pre-processed image-2, e) optic disc segmented image-1, f) optic disc segmented image-2, g) blood vessel segmented image-1, h) blood vessel segmented image-2, i) LGB feature image-1, j) LGB feature image-2, k) detected image-1, l) detected image-2*

4.3 Dataset Description

The IDRiD [20] database used in this research comprises segmentation, disease grading, and localization. The segmentation set has 81 images that are categorized as training and testing sets in JPG format; moreover, the ground images for the lesions are in TIF file format. The disease grading and localization contains 413 and 103 images in the training and testing test; moreover, ground truth labels in disease grading are in CSV format for disease grading, also ground truth labels in the localization phase are in CSV format for the localization set.

4.4 Evaluation Metric

The measures of LGAT-PCANet are described as follows:

4.4.1 Accuracy

It determines the accurate detected number of cases from overall test cases [21], which is expressed by,

$$Acc = \frac{Tr_{pos} + Tr_{neg}}{Tr_{pos} + Tr_{neg} + Fa_{pos} + Fa_{neg}} \tag{32}$$

4.4.2 Sensitivity

It calculates the number of exact positive cases from all positives [21] that is modeled by,

$$Sen = \frac{Tr_{pos}}{Tr_{pos} + Fa_{neg}} \tag{33}$$

4.4.3 Specificity

This quantifies the number of accurate negative cases from total negatives [21] using,

$$Spec = \frac{Tr_{neg}}{Tr_{neg} + Fa_{pos}} \tag{34}$$

Here, $Tr_{pos}, Tr_{neg}, Fa_{pos}, Fa_{neg}$ specifies true positive, true negative, false positive, and false negative.

4.5 Performance Evaluation

The assessment of LGAT-PCANet is done by changing training data based on epochs is evaluated in this section.

4.5.1 Analysis of LGAT-PCANet varying training data

In Fig. 4, the LGAT-PCANet evaluation is analyzed by differing training data based on epochs. Fig. 4 a) Designs LGAT-PCANet related to accuracy. With the 90% of training data, the LGAT-PCANet of accuracy attained for epochs 20 to 100 with 82.701%, 84.806%, 86.289%, 88.374% and 90.420%. In Fig. 4 b), the

LGAT-PCANet examination is carried out in accordance with sensitivity. If training data=90%, the sensitivity of LGAT-PCANet gained 82.333%, 83.353%, 85.999%, 87.500%, and 89.589% for epochs 20 to 100. Fig. 4 c) manifests the specificity of LGAT-PCANet. When training data is 90%, LGAT-PCANet reached 83.206%, 85.417%, 87.130%, 89.369%, and 91.433% for epochs 20 to 100.

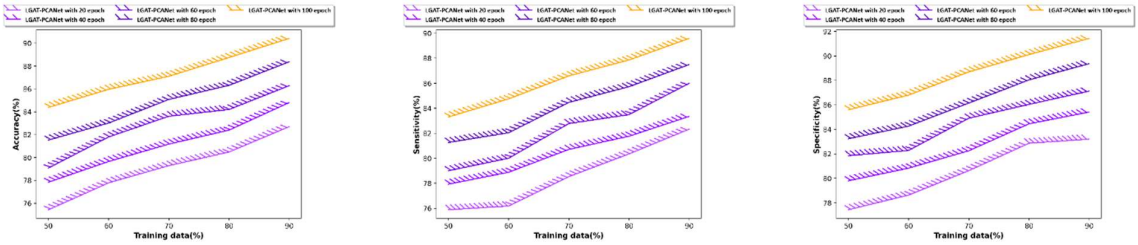

(a) (b) (c)

Fig. 4. *Analysis of LGAT-PCANet varying training data, a) Accuracy, b) Sensitivity, c) Specificity*

4.6 Comparative Methods

ADL-CNN [1], CDELM [2], EfficientNetB0 CNN [3], and DRNet13 [4] are the conventional modules for the proposed LGAT-PCANet.

4.7 Comparative Analysis

Here, LGAT-PCANet analysis is performed by training data, which is analyzed in the below sub-phases.

4.7.1 Analysis of LGAT-PCANet with training data

The comparative estimation of LGAT-PCANet is conducted with the different values of training data, which originated in Fig. 5. In Fig. 5 a), the analysis of LGAT-PCANet based on accuracy is designed. While training data is 90%, LGAT-PCANet in respect of accuracy obtained 90.315%, wherein performance gain of LGAT-PCANet observed by comparing the traditional approaches namely, ADL-CNN, CDELM, EfficientNetB0 CNN, and DRNet13 with the values of 8.592%, 6.716%, 4.771%, and 2.270%. Fig. 5 b) specifies the sensitivity of LGAT-PCANet analysis. The developed technique LGAT-PCANet obtained a sensitivity of 89.581% with training data as 90% while comparing the preceding techniques, the performance improvement of LGAT-PCANet is attained by 8.148%, 5.315%, 3.975%, and 2.489%. In Fig. 5 c), the LGAT-PCANet assessment for specificity. When training data is 90%, the LGAT-PCANet relating to specificity achieved 91.489%, whereas by comparing the traditional models, the performance enhancement of LGAT-PCANet obtained 7.587%, 5.776%, 3.808%, and 2.314%.

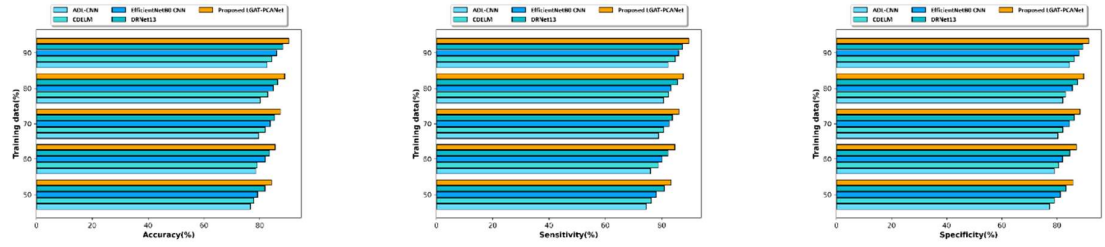

(a) (b) (c)

Fig. 5. *Analysis of LGAT-PCANet varying training data, a) Accuracy, b) Sensitivity, c) Specificity*

4.8 Comparative Discussions

Table 1 enumerates a comparative analysis discussion, in which LGAT-PCANet is evaluated with ADL-CNN, CDELM, EfficientNetB0 CNN, and DRNet13. Here, the accuracy of LGAT-PCANet gained 90.315%, which shows that the proposed approach is enable to detect the disease in an early stage with better generalizability. Moreover, the sensitivity of LGAT-PCANet achieved 89.581%, where which demonstrates that this model can easily evaluate and handle utilizing large volumes of data. Furthermore, the specificity of LGAT-PCANet acquired 91.489%, which expresses that the module is computationally efficient with high-speed convergence for the training process. Therefore, the LGAT-PCANet proves that it can attain high accuracy in detecting diabetic retinopathy at different stages and enhancing its performance over time.

Table 1. *Comparative Discussions*

Alteration based on	Metrics/Methods	ADL-CNN	CDELM	EfficientNetB0 CNN	DRNet13	Proposed LGAT-PCANet
Training data=50%	*Accuracy (%)*	76.666	77.826	79.185	81.797	84.160
	Sensitivity (%)	74.562	76.285	78.051	80.966	83.320
	Specificity (%)	77.314	79.040	81.252	83.257	85.814
Training data=90%	*Accuracy (%)*	82.555	84.249	86.006	88.265	**90.315**
	Sensitivity (%)	82.281	84.819	86.019	87.351	**89.581**
	Specificity (%)	84.548	86.205	88.005	89.373	**91.489**

5. Conclusion

Diabetic retinopathy is a severe complication of diabetes mellitus, which progressively damages the eye. Early detection is significant for preventing damage to the retina. Utilizing DL for predicting disease has enhanced over the last few years as more DL techniques are developed and combined into medical practice, which might be useful for specialists to treat patients in need effectively. An investigation related to diabetic retinopathy detection using retinal fundus image is designed with LGAT-PCANet. In this process, the input image is filtered by AWF in the image pre-processing phase. Moreover, optic disc and blood vessel segmentation is carried out by employing an active contour model and sparking process. Thereafter, feature extraction is done to extract the suitable features. Accordingly, the diabetic retinopathy detection phase is carried out by utilizing PCANet. The analytic metrics, like accuracy, sensitivity, and specificity obtained uttermost values of 90.315%, 89.581%, and 91.489%. Future work will develop a new color space model to enhance the characterization of complex visual patterns in retinal images.

Compliance With Ethical Standards

Conflicts of interest: Authors declared that they have no conflict of interest.

Human participants: The conducted research follows ethical standards and the authors ensured that they have not conducted any studies with human participants or animals.

References

[1] E. Ozbay, “An active deep learning method for diabetic retinopathy detection in segmented fundus images using artificial bee colony algorithm”, Artificial Intelligence Review, vol. 56, no. 4, pp.3291-3318, 2023.

[2] D.C.R. Novitasari, F. Fatmawati, R. Hendradi, H. Rohayani, R. Nariswari, A. Arnita, M. I. Hadi, R. A. Saputra, and A. Primadewi, “Image fundus classification system for diabetic retinopathy stage detection using hybrid CNN-DELM”, Big Data and Cognitive Computing, vol. 6, no. 4, pp.146, 2022.

[3] S. P. Singh, P. Gupta, and R. Dung, “Diabetic retinopathy detection by fundus images using fine tuned deep learning model”, Multimedia Tools and Applications, pp.1-23, 2024.

[4] F. J. M. Shamrat, R. Shakil, B. Akter, M. Z. Ahmed, K. Ahmed, F. M. Bui, and M. A. Moni, “An advanced deep neural network for fundus image analysis and enhancing diabetic retinopathy detection”, Healthcare Analytics, vol. 5, pp.100303, 2024.

[5] T. R. Athira, and J. J. Nair, “Diabetic retinopathy grading from color fundus images: an autotuned deep learning approach”, Procedia Computer Science, vol. 218, pp.1055-1066, 2023.

[6] G. Ali, A. Dastgir, M. W. Iqbal, M. Anwar, and M. Faheem, “A hybrid convolutional neural network model for automatic diabetic retinopathy classification from fundus images”, IEEE Journal of Translational Engineering in Health and Medicine, vol. 11, pp.341-350, 2023.

[7] W. L. Alyoubi, W. M. Shalash, and M. F. Abulkhair, “Diabetic retinopathy detection through deep learning techniques: A review”, Informatics in Medicine Unlocked, vol. 20, pp.100377, 2020.

[8] K. Verma, P. Deep, and A. G. Ramakrishnan, “Detection and classification of diabetic retinopathy using retinal images”, In proceedings of 2011 Annual IEEE India Conference, pp. 1-6, IEEE, December 2011.

[9] N. Tsiknakis, D. Theodoropoulos, G. Manikis, E. Ktistakis, O. Boutsora, A. Berto, F. Scarpa, A. Scarpa, D. I. Fotiadis, and K. Marias, “Deep learning for diabetic retinopathy detection and classification based on fundus images: A review”, Computers in biology and medicine, vol. 135, pp.104599, 2021.

[10] S. M. S. Islam, M. M. Hasan, and S. Abdullah, “Deep learning based early detection and grading of diabetic retinopathy using retinal fundus images”, arXiv preprint arXiv:1812.10595, 2018.

[11] F. Wu, W. Yang, L. Xiao, and J. Zhu, “Adaptive wiener filter and natural noise to eliminate adversarial perturbation”, Electronics, vol. 9, no. 10, pp.1634, 2020.

[12] A. S. Abdullah, J. Rahebi, Y. E. Özok, and M. Aljanabi, “A new and effective method for human retina optic disc segmentation with fuzzy clustering method based on active contour model”, Medical & biological engineering & computing, vol. 58, pp.25-37, 2020.

[13] V. M. Mane, and D. V. Jadhav, "Holoentropy enabled-decision tree for automatic classification of diabetic retinopathy using retinal fundus images", Biomedical Engineering/Biomedizinische Technik, vol. 62, no. 3, pp.321-332, 2017.
[14] W. Zhou, L. Yu, W. Qiu, Y. Zhou, and M. Wu, "Local gradient patterns (LGP): An effective local-statistical-feature extraction scheme for no-reference image quality assessment", Information Sciences, vol. 397, pp.1-14, 2017.
[15] L. Chen, D. Zhao, and F. Ge, "Image encryption based on singular value decomposition and Arnold transform in fractional domain", Optics Communications, vol. 291, pp.98-103, 2013.
[16] Y. Hatanaka, H. Tachiki, K. Ogohara, C. Muramatsu, S. Okumura, and H. Fujita, "Artery and vein diameter ratio measurement based on improvement of arteries and veins segmentation on retinal images", In proceedings of 2016 38th Annual International Conference of the IEEE Engineering in Medicine and Biology Society (EMBC), pp. 1336-1339, IEEE, August 2016.
[17] B. Esmael, A. Arnaout, R. Fruhwirth, and G. Thonhauser, "A statistical feature-based approach for operations recognition in drilling time series", International Journal of Computer Information Systems and Industrial Management Applications, vol. 4, no. 6, pp.100-108, 2012.
[18] O. Butusov, and V. Dikusar, "Image pattern analysis with image potential transform", Metody Ilosciowe w Badaniach Ekonomicznych, vol. 19, no. 1, pp.12-27, 2018.
[19] T. H. Chan, K. Jia, S. Gao, J. Lu, Z. Zeng, and Y. Ma, "PCANet: A simple deep learning baseline for image classification?", IEEE transactions on image processing, vol. 24, no. 12, pp.5017-5032, 2015.
[20] Indian Diabetic Retinopathy Image Dataset (IDRiD) database taken from "https://ieee-dataport.org/open-access/indian-diabetic-retinopathy-image-dataset-idrid" accessed on October 2024.
[21] M. Sharma, Monika, N. Kumar, and P. Kumar, "Badminton match outcome prediction model using Naïve Bayes and Feature Weighting technique", Journal of Ambient Intelligence and Humanized Computing, vol. 12, pp.8441-8455, 2021.